

# The 2D NMR Experiments $H(C)CO_2$ and $H\underline{C}CO_2$ for Assignment and pH Titration of Carboxylate Groups in Uniformly $^{15}N/^{13}C$ -Labeled Proteins

MAURIZIO PELLECCIA, HIDEO IWAI, THOMAS SZYPERSKI, AND KURT WÜTHRICH

*Institut für Molekularbiologie und Biophysik, Eidgenössische Technische Hochschule-Hönggerberg, CH-8093 Zürich, Switzerland*

Received November 8, 1996

In the practice of assigning the  $^1H$  NMR spectra of proteins as a basis for three-dimensional structure determination (1), unique and complete identification of the amino-acid side-chain spin systems remains a limiting factor. When using homonuclear  $^1H$  NMR, only 6 out of the 20 proteinogenic amino acids can be uniquely assigned from the symmetry of the spin systems of the nonlabile hydrogen atoms (2), and early attempts at editing the  $^1H$  NMR spectra for unique  $^1H$  spin system types (3) found little practical use. In uniformly  $^{13}C/^{15}N$ -labeled proteins studied in solvents where the labile side-chain amide protons are observable, unique scalar coupling patterns can be outlined for all common amino acids, with the possible exception of the residue pair Ser and Cys. To expand the existing arsenal of experiments capable of identifying the complete spin systems in the highly complex protein NMR spectra, this Communication presents two-dimensional triple-resonance NMR experiments for identification of the acidic side-chain spin systems by selective correlation of  $^{13}CH_2^\beta$  and  $^{13}CO_2^\gamma$  of Asp, and  $^{13}CH_2^\gamma$  and  $^{13}CO_2^\delta$  of Glu, and of the C-terminal residue by selective correlation of  $^{13}CH^\alpha$  with  $^{13}CO_2$ . Since these experiments, named 2D  $H(C)CO_2$  and 2D  $H\underline{C}CO_2$ , specifically select for  $^{13}CO_2$ , they yield greatly simplified spectra. In addition to the use for resonance assignments, an attractive application is for the determination of the carboxylate  $pK_a$  values in investigations of structural roles of the acidic side chains (4, 5) and their participation in functionally active sites.

The experiments described presently are an addition to a group of measurements previously introduced for identification of different amino acid side chains, which filter the resonances of selected amino acids on the basis of unique spin-spin scalar couplings (6–10). Quite naturally, as pointed out by Gehring and Guittet (9), the resulting spectra are sparsely populated with peaks and therefore particularly suited for a reduction in dimensionality by use of the recently published projection technique (11, 12). The pulse scheme of the 2D  $H\underline{C}CO_2$  experiment (Fig. 1; the underlined letters indicate that  $^{13}CO_2$  and its directly attached  $^{13}C$  spins evolve

simultaneously as single-quantum coherence and are observed in a common dimension;  $CO_2$  is used to express that carboxylates are selectively observed) is derived from the 3D ct-HCACO experiment (13, 14) designed for backbone-resonance assignments. The 2D  $H(C)CO_2$  experiment is obtained with the same pulse scheme when the  $^{13}C^{\beta/\gamma}$  chemical-shift evolution is omitted by setting the factor  $\kappa$  to zero (Fig. 1). In the following product-operator description (15), only terms resulting in observable magnetization during the detection period are retained and constant multiplicative factors and trigonometric terms are omitted. Pulsed field gradients (PFG) are employed for coherence pathway rejection and water suppression (16, 17). For simplicity, the transfer amplitude will be derived for an Asp residue with degenerate  $^1H^\beta$  chemical shifts. The spin operators for  $^1H^\beta$ ,  $^{13}C^\beta$ , and  $^{13}CO_2$  are denoted as  $I$ ,  $C$ , and  $C'$ . The experiment starts with an INEPT transfer of polarization from protons to carbons, so that at time  $a$  (Fig. 1) we have transverse  $^{13}C^\beta$  magnetization in antiphase with respect to one of the attached protons,

$$\sigma(a) = C_y I_z. \quad [1]$$

This magnetization is refocused during  $\tau_2 = \frac{1}{4} \{^1J_{CH}\}$  (18). Then, the  $^{13}C^\beta$  magnetization is transferred to the adjacent  $^{13}CO_2$  group during  $\tau_3$ . To minimize losses due to dephasing caused by the passive  $^1J(^{13}C^\alpha, ^{13}C^\beta)$  coupling,  $\tau_3$  is set to 7.2 ms (13, 14). The magnetization before the first  $90^\circ$  pulse on  $^{13}CO_2$  is thus described by  $C_y C'_z$ . Between the time points  $a$  and  $b$ , the  $^{13}CO_2$  and  $^{13}C^\beta$  chemical shifts evolve during the times  $t_1$  and  $\kappa \times t_1$  (in a constant time fashion), respectively, so that the magnetization at point  $b$  (Fig. 1) is

$$\begin{aligned} \sigma(b) &= C_y C'_z \{ \cos[\Omega(^{13}C^\beta)\kappa \times t_1] \cos[\Omega(^{13}CO)t_1] \}. \quad [2] \end{aligned}$$

During the  $^{13}CO_2$  chemical-shift evolution,  $^{13}C^\beta$  is decoupled by a  $180^\circ$  pulse. In contrast to the Asp resonances, the scalar

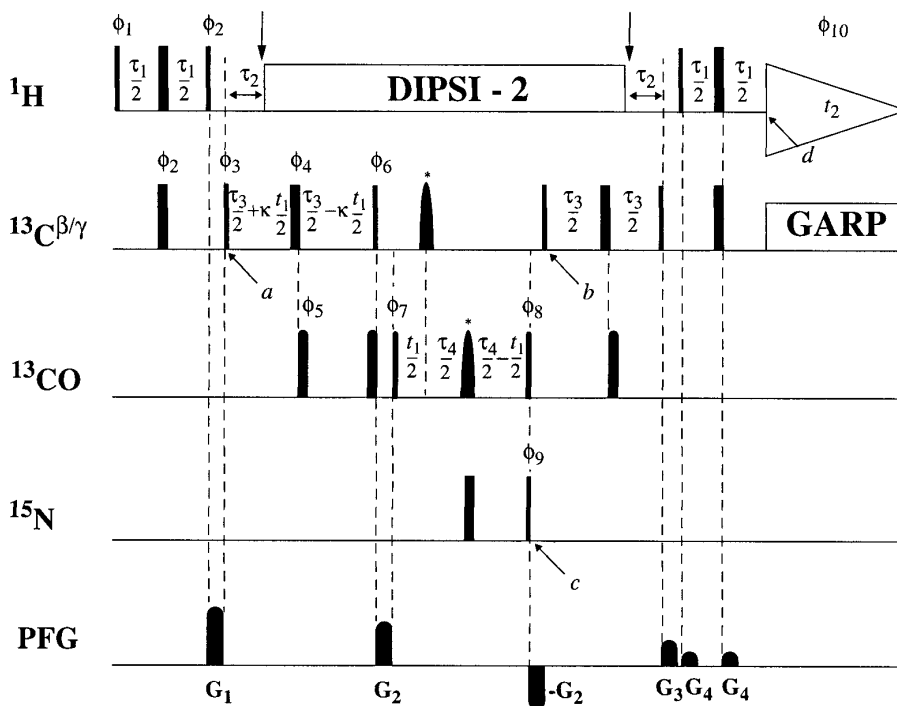


**FIG. 1.** Experimental scheme of the 2D  $\text{HCCO}_2$  experiment. Ninety degree and  $180^\circ$  pulses are indicated by thin and thick vertical bars, respectively. Where no RF phase is marked, the pulse is applied along  $x$ ; otherwise, the phases are indicated above the pulses. For the present project, we used the following conditions: The carrier for the first three  $^1\text{H}$  pulses is placed on the solvent line at 4.9 ppm; then it is switched to 2.5 ppm for the duration of the DIPSI-2 sequence (34), and subsequently it is switched back to 4.9 ppm (the two vertical arrows indicate the time points at which the offset is switched). The  $^{13}\text{C}^{\beta/\gamma}$  and  $^{15}\text{N}$  carriers are set to 40 and 110 ppm, respectively. The  $90^\circ$  pulse lengths are  $12\ \mu\text{s}$  for  $^1\text{H}$ ,  $40\ \mu\text{s}$  for  $^{15}\text{N}$ ,  $47\ \mu\text{s}$  for  $^{13}\text{C}^{\beta/\gamma}$ , and  $92\ \mu\text{s}$  for  $^{13}\text{CO}$ . The corresponding  $180^\circ$  pulses are applied with the same power. The pulses on  $^{13}\text{CO}$  have the shape of a sinc center lobe applied in a phase-modulated manner with the center of excitation at 180 ppm, and they have been optimized to avoid excitation of  $^{13}\text{C}^{\beta/\gamma}$  magnetization. A  $^{13}\text{CO}$  RE-BURP pulse (35) of  $400\ \mu\text{s}$  and  $15.7\ \text{kHz}$  peak amplitude and a  $^{13}\text{C}^{\beta/\gamma}$  I-BURP2 pulse (35) of  $400\ \mu\text{s}$  and  $12.4\ \text{kHz}$  peak amplitude are applied during the  $^{13}\text{CO}$  evolution period (these two pulses are identified with asterisks). The pulse length for  $^{13}\text{C}^{\beta/\gamma}$  and  $^{13}\text{CO}$  have been optimized for a  $^1\text{H}$  frequency of 600 MHz and the  $^{13}\text{C}^{\beta/\gamma}$  and  $^{13}\text{CO}$  carrier positions given above, using the Varian program *Pulsetool*. The  $^{13}\text{C}^{\beta/\gamma}$  and  $^{13}\text{CO}$  pulses could not be applied simultaneously because they are generated by the same RF channel. The duration and amplitudes of the sine-bell-shaped PFGs are 1 ms and 60 G/cm for  $G_1$ , 1 ms and 40 G/cm for  $G_2$ , 1 ms and 20 G/cm for  $G_3$ , and  $200\ \mu\text{s}$  and 8 G/cm for  $G_4$ . The delays are  $\tau_1 = 3.0\ \text{ms}$ ,  $\tau_2 = 1.6\ \text{ms}$ ,  $\tau_3 = 7.2\ \text{ms}$ , and  $\tau_4 = 32\ \text{ms}$ .  $\kappa$  represents a scaling factor for the chemical-shift evolution of  $^{13}\text{C}^{\beta/\gamma}$  (see text). The 2D  $\text{H}(\text{C})\text{CO}_2$  experiment is recorded by setting  $\kappa = 0$  (see text). The phase cycling for the pulse scheme is  $\phi_1 = y$ ;  $\phi_2 = x, -x$ ;  $\phi_3 = x$ ;  $\phi_4 = 8x, 8y, 8(-x), 8(-y)$ ;  $\phi_5 = 8x, 8(-x)$ ;  $\phi_6 = 4x, 4(-x)$ ;  $\phi_7 = x, x, -x, -x$ ;  $\phi_8 = x, -x$ ;  $\phi_9 = x$ ;  $\phi_{10}$  (receiver) =  $2x, 4(-x), 2x, 2(-x), 4x, 2(-x)$ . Quadrature detection in  $t_1$  is accomplished by altering the phase  $\phi_7$  according to States-TPPI (19). To shift the apparent  $^{13}\text{C}^{\beta/\gamma}$  carrier position to 48.5 ppm in the 2D  $\text{HCCO}_2$  experiment, the phase  $\phi_3$  is incremented in  $40^\circ$  steps according to TPPI (20–22). The magnetization transfer obtained from the pulse scheme was analyzed using the product-operator formalism (15) implemented in the program POMA (36). A DIPSI-2 sequence (34) with  $\text{RF} = 1.2\ \text{kHz}$  is used to decouple  $^1\text{H}$  during the heteronuclear magnetization transfer, and a GARP sequence (37) with  $\text{RF} = 1.0\ \text{kHz}$  is employed to decouple  $^{13}\text{C}^{\beta/\gamma}$  during  $t_2$ .

coupling between  $^{13}\text{CO}^\gamma$  and  $^{15}\text{N}^\delta$  of Asn evolves during  $\tau_4 = \frac{1}{2}\{^1J_{\text{CON}}\}$ , yielding transverse  $^{13}\text{CO}$  magnetization in anti-phase with respect to the attached  $^{15}\text{N}$  and  $^{13}\text{C}$  spins. At time point  $c$  (Fig. 1), the two pulses denoted  $\phi_8$  and  $\phi_9$  in Fig. 1 then generate a product-operator term of the form  $C_z C'_x N_y$ , where the spin operator  $N$  represents  $^{15}\text{N}^\delta$ . This heteronuclear two-spin coherence is dephased by the subsequent gradient ( $-G_2$  in Fig. 1). The  $90^\circ$  pulse on  $^{13}\text{C}^{\beta/\gamma}$  just before point  $b$  then generates a three-spin coherence of the form  $C_y C'_x N_y$ , which does not refocus to observable magnetization, so that the cross peaks from Asn are eliminated from the 2D spectrum. The magnetization transfer described here for the side-chain  $-\text{CH}_2-\text{CO}-\text{NH}_2$  moieties likewise occurs

for the backbone fragments  $-\text{CH}-\text{CO}-\text{NH}-$ , whose cross peaks are therefore also eliminated. For Asp, the subsequent INEPT-type back transfer of antiphase  $^{13}\text{CO}_2$  magnetization via  $^{13}\text{C}^\beta$  to  $^1\text{H}^\beta$  occurs during  $\tau_3$  and  $\tau_1$ , so that the observable magnetization at the start of the acquisition ( $d$  in Fig. 1) is given by

$$\sigma(d) = I_x \{ \cos[\Omega(^{13}\text{C}^\beta)\kappa \times t_1] \cos[\Omega(^{13}\text{CO}_2)t_1] \}. \quad [3]$$

Analogous results are obtained for Glu and for the C-terminal residue. The phase error caused by an off-resonance effect arising from the first  $180^\circ$  ( $^{13}\text{CO}$ ) pulse on the transverse  $^{13}\text{C}^{\beta/\gamma}$  magnetization is eliminated by a second  $180^\circ$

pulse on  $^{13}\text{CO}$  (Fig. 1) (14). As described previously in the context of two-spin coherence spectroscopy (12),  $\sigma(d)$  contains the sum and the difference of the chemical shifts of  $^{13}\text{C}^{\beta/\gamma}$  and  $^{13}\text{CO}_2$ , which can be detected in a phase-sensitive manner by applying the States–TPPI method (19) to either  $^{13}\text{C}^{\beta/\gamma}$  or  $^{13}\text{CO}_2$ . Here, States–TPPI was applied to  $^{13}\text{CO}_2$ , yielding for Asp resonances at  $\Omega(^{13}\text{CO}_2^\gamma) \pm \kappa\Omega(^{13}\text{C}^\beta)$ , for Glu at  $\Omega(^{13}\text{CO}_2^\delta) \pm \kappa\Omega(^{13}\text{C}^\gamma)$ , and for the C-terminus at  $\Omega(^{13}\text{CO}_2^\epsilon) \pm \kappa\Omega(^{13}\text{C}^\alpha)$ .

In 2D  $\text{HCCO}_2$  with  $\kappa = 1$ , the delay  $\tau_3 = 7.2$  ms is too short to adequately exploit  $\tau_4 = 32$  ms for  $^{13}\text{CO}_2$  frequency labeling (Fig. 1). We therefore set the increment for  $^{13}\text{C}^{\beta/\gamma}$  to  $\kappa = 0.35$ . As a consequence, the  $^{13}\text{C}^{\beta/\gamma}$  chemical shift and thus the in-phase splitting of the  $^{13}\text{CO}_2$  signals are scaled down by  $\kappa$ . Since the  $^{13}\text{C}^{\beta/\gamma}$  chemical shifts are extracted from the difference between peaks at  $\Omega(^{13}\text{CO}_2) \pm \kappa\Omega(^{13}\text{C}^{\beta/\gamma})$ , the carrier for pulses applied to  $^{13}\text{C}^{\beta/\gamma}$  must, in principle, be set at the edge of the  $^{13}\text{C}^{\beta/\gamma}$  spectral range to obtain unambiguous  $^{13}\text{C}^{\beta/\gamma}$  assignments (11, 12). However, to minimize off-resonance effects, we placed the  $^{13}\text{C}^{\beta/\gamma}$  carrier in the center of this spectral range and employed time-proportional phase incrementation (TPPI) (20–22) on  $\phi_3$  (Fig. 1). Since in the 2D  $\text{HCCO}_2$  experiment the  $^{13}\text{CO}_2$  and  $^{13}\text{C}^{\beta/\gamma}$  chemical shifts are both encoded during constant-time evolution periods, the resulting modulation of the transfer function along  $t_1$  has a constant amplitude and is therefore particularly amenable to linear prediction (23).

In general,  $^1\text{H}$ – $^{13}\text{CO}$  correlations for side-chain resonances can be obtained with an adapted version of the 2D ct-H(CA)CO experiment (24, 25). As in the 2D H(C)CO<sub>2</sub> and the 2D  $\text{HCCO}_2$  pulse schemes (Fig. 1), transverse  $^{13}\text{C}^{\beta/\gamma}$  magnetization is present for only 14 ms, making it a rather sensitive experiment. However, in both 2D H(C)CO<sub>2</sub> and 2D  $\text{HCCO}_2$  (Fig. 1), additional losses occur during the constant-time delay  $\tau_4 = 32$  ms which is needed to eliminate cross peaks from Asn and Gln, but due to the relatively long  $T_2$  values for  $^{13}\text{CO}_2$ , the signal attenuation is quite small (about a factor 1.4 for our protein). In the 2D  $\text{HCCO}_2$  experiment, an additional loss in sensitivity of a factor 2 is due to the in-phase splitting of the peaks. There is also a COCAH “out-and-stay” experiment (26) which does not use the first two INEPT-type transfer steps of H(CA)CO but starts with a  $90^\circ$  pulse on  $^{13}\text{CO}_2$ . Although this pulse scheme promises significantly reduced losses due to passive spin–spin couplings, transverse relaxation, and pulse imperfections, the “out-and-back” 2D H(C)CO<sub>2</sub> experiment is superior since it transfers the steady-state magnetization of two protons in the  $\text{CH}_2^{\beta/\gamma}$  group instead of the single  $^{13}\text{CO}_2$  steady-state magnetization used in the out-and-stay scheme. Furthermore,  $T_1$ -relaxation times are usually much shorter for  $^1\text{H}^{\beta/\gamma}$  than for  $^{13}\text{CO}_2$  which also speaks in favor of the out-and-back version implemented here. Hence, the 2D  $\text{HCCO}_2$  experiment of Fig. 1 appears to be the preferred option for identification of Asp, Glu, and the C-terminus in proteins.

As a practical application, we recorded 2D H(C)CO<sub>2</sub> (Fig. 2B) and 2D  $\text{HCCO}_2$  spectra (Fig. 2C) of a 1 mM solution of the  $^{13}\text{C}$ ,  $^{15}\text{N}$  doubly labeled 63-residue N-terminal domain of the 434 repressor [434(1–63)], a protein with molecular weight 6900. For comparison, we also recorded a 2D ct-H(CA)CO experiment adapted for side-chain correlation (25) (Fig. 2A). The measurements were performed at  $13^\circ\text{C}$ . At this temperature, the protein reorients with a correlation time of about 5.6 ns (P. Luginbühl, K. Pervushin, H. Iwai, and K. Wüthrich, to be published), so that spectral data of comparable quality can be expected for proteins with molecular weight up to about 15,000 when recorded at temperatures around  $30^\circ\text{C}$ . In the 2D ct-H(CA)CO spectrum (Fig. 2A), all correlations between  $^1\text{H}^\beta$  and  $^{13}\text{CO}^\gamma$  of Asp57, Asn16, Asn36, and Asn61 as well as the correlations between  $^1\text{H}^\gamma$  and  $^{13}\text{CO}^\delta$  of the Glu residues in positions 19, 32, 35, and 47 and the Gln residues 12, 17, 22, 28, 29, and 33 are observed. In the 2D H(C)CO<sub>2</sub> spectrum (Fig. 2B), only the cross peaks corresponding to Asp and Glu are selected (weak cross peaks from the C-terminal residue were observed outside of the spectral region shown). In particular, the assignment of the side-chain carboxyl carbon of Asp57 in the 2D ct-H(CA)CO spectrum is ambiguous because of overlap with the resonances of Gln 33 (Fig. 2A). This overlap, and thus the assignment ambiguity, is neatly resolved in Fig. 2B. Moreover, elimination of signals arising from Asn and Gln residues notably reduces the total number of cross peaks, making this experiment ideally suited for use of the projection technique (11, 12) that yields the 2D  $\text{HCCO}_2$  spectrum of Fig. 2C, which in addition provides the  $^{13}\text{C}^{\beta/\gamma}$  chemical shifts.

The side-chain carboxylates of Asp and Glu residues are frequently involved in catalytic centers of enzymes, in salt bridges, and in hydrogen bonds. Their identification and the determination of their  $\text{pK}_a$  values is important to understand the mechanisms of catalytic reactions as well as the contributions of these groups to the stability of proteins by formation of salt bridges and hydrogen bonds, and in particular to characterize transient hydrogen-bonding interactions on the protein surface (4, 5). Recently, 2D ct-H(CA)CO adapted to detect side-chain  $^{13}\text{CO}$  resonances (25) has been used to determine  $\text{pK}_a$  values for the carboxyl groups in  $^{15}\text{N}/^{13}\text{C}$ -labeled proteins (e.g., 27–30). The 2D H(C)CO<sub>2</sub> and the 2D  $\text{HCCO}_2$  experiments presented in this Communication greatly reduce the problem of spectral overlap when compared with 2D ct-H(CA)CO (see Fig. 2) and thus circumvent the necessity to produce selectively  $^{13}\text{CO}_2$ -labeled samples (e.g., 31–33). Since it also provides correlations with  $^{13}\text{C}^{\beta/\gamma}$ , 2D  $\text{HCCO}_2$  is most informative for obtaining the resonance assignments, whereas 2D H(C)CO<sub>2</sub> is the preferred experiment for pH titrations of the carboxylate groups. Normally, there is hardly any interference between the resonances of the side-chain carboxylates of Asp and Glu and the C-terminus, and good conditions for observation of the

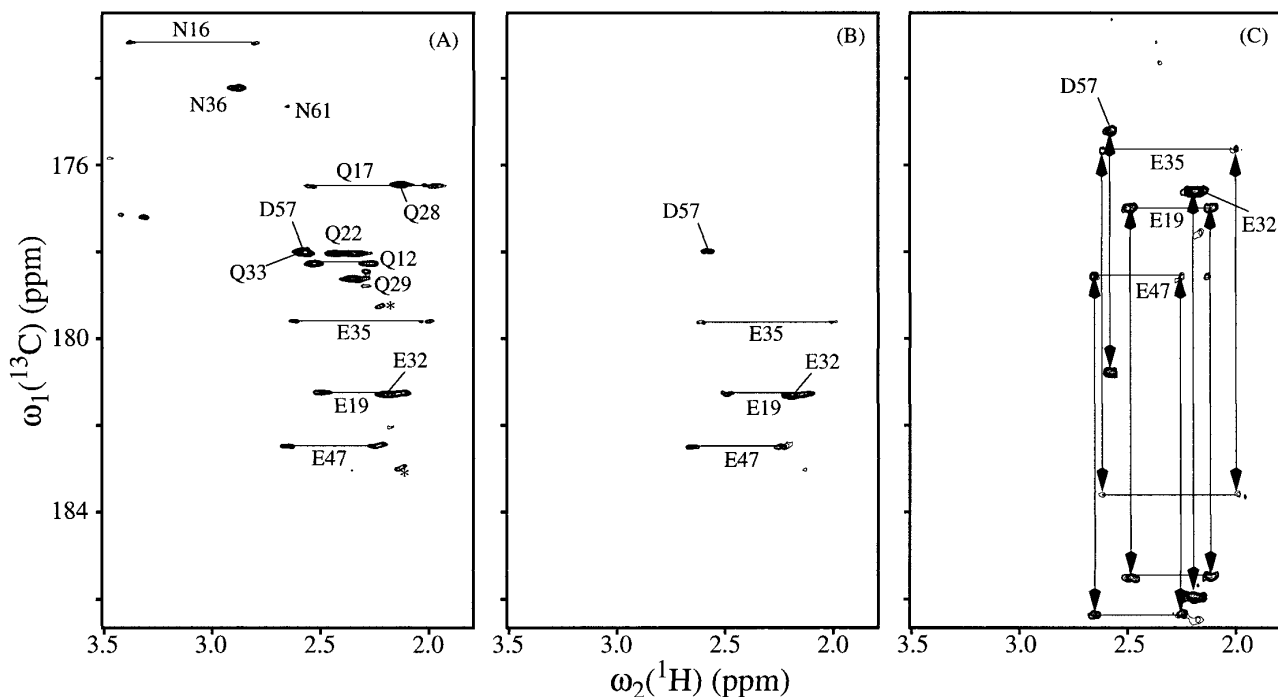


**FIG. 2.** Spectra obtained with a 1 mM sample of uniformly  $^{13}\text{C}/^{15}\text{N}$ -labeled 434(1-63) (solvent  $\text{D}_2\text{O}$ ,  $\text{pD}^* 7.0$ ,  $T = 13^\circ\text{C}$ ). The spectra were recorded on a Bruker AMX 600 spectrometer operating at 600 MHz  $^1\text{H}$  frequency. (A) Two-dimensional ct-H(CA)CO (24) adapted for the observation of side-chain correlations (25). The spectrum was acquired with  $180(t_1) \times 1024(t_2)$  complex points with  $t_{1\text{max}}(^{13}\text{CO}) = 43.2$  ms, and  $t_{2\text{max}}(^1\text{H}) = 131$  ms. The digital resolution after zero-filling was 8 Hz along  $\omega_1(^{13}\text{CO})$  and 7.6 Hz along  $\omega_2(^1\text{H})$ . The total measuring time was about 6 h. Backbone  $-\text{CH}-\text{CO}-\text{N}-$  transfers lead to additional cross peaks. However, because  $^1\text{H}^\alpha$  usually resonates downfield from  $^1\text{H}^{\beta/\gamma}$  of Asp and Glu (2), most of these additional cross peaks do not appear in the spectral region of interest. (B) Two-dimensional H(C)CO $_2$ ,  $90(t_1) \times 1024(t_2)$  complex points were accumulated with  $t_{1\text{max}}(^{13}\text{CO}) = 21.6$  ms,  $t_{2\text{max}}(^1\text{H}) = 131$  ms, total measuring time about 6 h. (C) Two-dimensional HCCO $_2$ ,  $64(t_1) \times 1024(t_2)$  complex points were accumulated, and the scaling factor  $\kappa$  was set to 0.35, so that  $t_{1\text{max}}(^{13}\text{C}^{\beta/\gamma}) = 5.4$  ms and  $t_{1\text{max}}(^{13}\text{CO}) = 15.4$  ms,  $t_{2\text{max}}(^1\text{H}) = 131$  ms, total measuring time about 8 h. Phase-sensitive detection was achieved using the States-TPPI method (19) in  $t_1$  on  $^{13}\text{CO}$ , so that the peak positions along  $\omega_1$  are at  $\Omega(^{13}\text{CO}) \pm \kappa\Omega(^{13}\text{C}^{\beta/\gamma})$ . The apparent  $^{13}\text{C}^{\beta/\gamma}$  carrier position was shifted to 48.5 ppm by incrementing the phase  $\phi_3$  (Fig. 1) in  $40^\circ$  steps according to TPPI (20–22). The final data size of the experiments in (B, C) was doubled in  $t_1$  by linear prediction, resulting in a digital resolution, after zero-filling, of 8 Hz along  $\omega_1(^{13}\text{CO})$  and 7.6 Hz along  $\omega_2(^1\text{H})$ . All spectra were processed using the program PROSA (38) and analyzed with the program XEASY (39). The assignments of the individual carboxyl and carbonyl resonances obtained on the basis of previous  $^1\text{H}$  assignments (40) are indicated. In (A), asterisks indicate cross peaks arising from an impurity. In (C), resonance assignments for  $^{13}\text{C}^\beta$  of Asp57 (40.5 ppm) and  $^{13}\text{C}^\gamma$  of Glu19 (36.4 ppm), Glu32 (35.2 ppm), Glu35 (37.2 ppm), and Glu47 (37.3 ppm) have been calculated in ppm from the in-phase splitting of the  $^{13}\text{CO}$  resonances according to  $\delta(^{13}\text{C}^{\beta/\gamma}) = \{\delta(^{13}\text{C})\text{-carr}\} - \Delta/2\kappa$ , where  $\Delta$  is the in-phase splitting along  $\omega_1$  in ppm, and  $\delta(^{13}\text{C})\text{-carr}$  represents the apparent  $^{13}\text{C}^{\beta/\gamma}$  carrier frequency in ppm.

latter are best obtained in separate experiments with newly optimized selection of the experimental parameters.

### ACKNOWLEDGMENTS

Financial support was obtained from the Schweizerischer Nationalfonds (Project 31.32033.91). We thank Dr. G. Wider for helpful discussions and Mrs. E. Ulrich for the careful processing of the manuscript.

### REFERENCES

1. K. Wüthrich, G. Wider, G. Wagner, and W. Braun, *J. Mol. Biol.* **155**, 311 (1982).
2. K. Wüthrich, "NMR of Proteins and Nucleic Acids," Wiley, New York, 1986.
3. M. H. Levitt and R. R. Ernst, *Chem. Phys. Lett.* **100**, 119 (1983).
4. A. Bundi and K. Wüthrich, *Biopolymers* **18**, 299 (1979).
5. T. Szyperski, W. Antuch, M. Schick, A. Betz, S. R. Stone, and K. Wüthrich, *Biochemistry* **33**, 9303 (1994).
6. S. Grzesiek and A. Bax, *J. Biomol. NMR* **3**, 185 (1993).
7. M. Wittekind, W. Metzler, and L. Müller, *J. Magn. Reson. B* **101**, 214 (1993).
8. E. T. Olejniczak and S. W. Fesik, *J. Am. Chem. Soc.* **116**, 2215 (1994).
9. K. Gehring and E. Guittet, *J. Magn. Reson. B* **109**, 206 (1995).
10. V. Dötsch, R. E. Oswald, and G. Wagner, *J. Magn. Reson. B* **110**, 107 (1996).
11. T. Szyperski, G. Wider, J. H. Bushweller, and K. Wüthrich, *J. Am. Chem. Soc.* **115**, 9307 (1993).
12. T. Szyperski, G. Wider, J. H. Bushweller, and K. Wüthrich, *J. Biomol. NMR* **3**, 127 (1993).

13. R. Powers, A. M. Gronenborn, G. M. Clore, and A. Bax, *J. Magn. Reson.* **94**, 209 (1991).
14. S. Grzesiek and A. Bax, *J. Magn. Reson. B* **102**, 103 (1993).
15. O. W. Sørensen, G. W. Eich, M. H. Levitt, G. Bodenhausen, and R. R. Ernst, *Prog. NMR Spectrosc.* **16**, 163 (1983).
16. A. Bax and S. S. Pochapsky, *J. Magn. Reson.* **99**, 638 (1992).
17. G. Wider and K. Wüthrich, *J. Magn. Reson. B* **102**, 239 (1993).
18. D. P. Burum and R. R. Ernst, *J. Magn. Reson.* **39**, 163 (1980).
19. D. Marion, M. Ikura, R. Tschudin, and A. Bax, *J. Magn. Reson.* **85**, 393 (1989).
20. D. Marion and K. Wüthrich, *Biochem. Biophys. Res. Commun.* **113**, 967 (1983).
21. B. Brutscher, J. P. Simorre, M. S. Caffrey, and D. Marion, *J. Magn. Reson. B* **105**, 77 (1994).
22. T. Szyperski, D. Braun, C. Fernández, C. Bartels, and K. Wüthrich, *J. Magn. Reson. B* **108**, 197 (1995).
23. D. S. Stephenson, *Prog. NMR Spectrosc.* **20**, 516 (1988).
24. L. E. Kay, M. Ikura, R. Tschudin, and A. Bax, *J. Magn. Reson.* **88**, 496 (1990).
25. T. Yamazaki, M. Yoshida, and K. Nagayama, *Biochemistry* **32**, 5656 (1993).
26. K. Dijkstra, G. J. Kroon, N. A. J. van Nuland, and R. M. Scheek, *J. Magn. Reson. A* **107**, 102 (1994).
27. M.-F. Jeng and H. J. Dyson, *Biochemistry* **35**, 1 (1996).
28. Y. Oda, T. Yamazaki, K. Nagayama, S. Kanaya, Y. Kuroda, and H. Nakamura, *Biochemistry* **33**, 5275 (1994).
29. Y. X. Wang, D. I. Freedberg, T. Yamazaki, P. T. Wingfield, S. J. Stahl, J. D. Kaufman, Y. Kiso, and D. Torchia, *Biochemistry* **35**, 9945 (1996).
30. J. Qin, G. M. Clore, and A. M. Gronenborn, *Biochemistry* **35**, 7 (1995).
31. D. E. Anderson, J. Lu, L. McIntosh, and F. W. Dahlquist, in "NMR of Proteins," p. 258, MacMillan, London, 1993.
32. D. E. Anderson, W. J. Becktel, and F. W. Dahlquist, *Biochemistry* **29**, 2403 (1990).
33. L. P. McIntosh, G. Hand, P. E. Johnson, M. D. Joshi, M. Körner, L. A. Plesniak, L. Zisen, W. W. Wakarchuk, and S. G. Withers, *Biochemistry* **35**, 9958 (1996).
34. A. J. Shaka, C. J. Lee, and A. J. Pines, *J. Magn. Reson.* **77**, 274 (1988).
35. H. Geen and R. Freeman, *J. Magn. Reson.* **93**, 93 (1991).
36. P. Güntert, N. Schäfer, G. Otting, and K. Wüthrich, *J. Magn. Reson. A* **101**, 103 (1993).
37. A. J. Shaka, P. B. Barker, and R. Freeman, *J. Magn. Reson.* **64**, 547 (1985).
38. P. Güntert, V. Dötsch, G. Wider, and K. Wüthrich, *J. Biomol. NMR* **2**, 619 (1992).
39. C. Bartels, T. H. Xia, M. Billeter, P. Güntert, and K. Wüthrich, *J. Biomol. NMR* **6**, 1 (1995).
40. D. Neri, M. Billeter, and K. Wüthrich, *J. Mol. Biol.* **223**, 743 (1992).